Tuning roughness and gloss of powder coating paint by encapsulating the coating particles with thin Al_2O_3 films

Valdesueiro, David; Hettinga, Hans; Drijfhout, Jan Pieter; Lips, Priscilla; Meesters, Gabrie M.H.; Kreutzer, Michiel T.; van Ommen, J.R.

DOI
10.1016/j.powtec.2017.05.019

Publication date
2017

Document Version
Final published version

Published in
Powder Technology

Powder Technology 318 (2017) 401–410

Contents lists available at ScienceDirect

Powder Technology

journal homepage: www.elsevier.com/locate/powtec

Tuning roughness and gloss of powder coating paint by encapsulating the coating particles with thin Al_2O_3 films

David Valdesueiro [a,c], Hans Hettinga [b], Jan Pieter Drijfhout [b], Priscilla Lips [b], Gabrie M.H. Meesters [a], Michiel T. Kreutzer [a], J. Ruud van Ommen [a,*]

[a] Delft University of Technology, Department of Chemical Engineering, Van der Maasweg 9, 2629, HZ, Delft, The Netherlands
[b] DSM Coating Resins, Ceintuurbaan 5, 8022 AW, Zwolle, The Netherlands
[c] Delft IMP B.V., Molengraaffsingel 10, 2629 JD, Delft, The Netherlands

ARTICLE INFO

Article history:
Received 27 June 2016
Received in revised form 10 April 2017
Accepted 11 May 2017
Available online 26 May 2017

Keywords:
Alumina coating
Core-shell particles
Ambient conditions
Atomic layer deposition
Matte powder coating
Surface appearance

ABSTRACT

In this work, we report a method to change the surface finish of a standard polyester-based powder coating paint, from gloss to matt, by depositing ultrathin films of Al_2O_3 on the powder coating particles. The coating experiments were performed in a fluidized bed reactor at 1 bar and 27 °C, using a gas-phase coating process of alternating exposure of the particles to the two precursors (trimethylaluminium and water), similar to atomic layer deposition (ALD). We varied the number of coating cycles (1, 2, 3, 5, 7 and 9 cycles) to obtain film thicknesses of the alumina shell ranging from 1 to 30 nm. The average growth per cycle of the process is 3.5 nm, significantly larger than the one for pure self-limiting ALD. When the average alumina shell was thicker than 6 nm, the shell prevented the flow of the core particles, even though the powder particles did soften above the glass transition temperature. With the particles morphology intact, this resulted in a rough and matte surface finish of the coating after curing. The surface roughness, with a value around 9 μm determined by surface profilometry, is associated to the alumina coated particles as observed with SEM and EDX analysis. In addition, the matte finish coating showed mechanical resistance similar to that of uncoated powder particles.

1. Introduction

A powder coating is a solvent-free powder-based type of coating used commonly to coat metals for a wide range of applications, such as in automotive industry. The surface appearance can be generally tuned by the addition of external additives to the powder formulation. Powder coatings have important advantages over liquid-based paints: being ease of application, high utilization by electrostatic spraying, environmentally friendly since they do not contain organic solvents, and showing excellent performance once applied. These strong points are also known as the *Four E's*, standing for ecology, excellence of finish, economy and energy [1–3]. These properties allow powder coatings to be used in a wide variety of applications, i.e. automotive, architectural, electronics and furniture amongst others [3]. A powder coating is composed of a resin, a catalyst, a cross-linker, pigments and additives such as flow modifiers and degassing agents, which define the properties of the final powder coating, including the surface finish (glossy or matte).

Glossy coatings reflect all the incident light in a mirror-like fashion, whereas a matte finish scatters part of the light, reducing the gloss level. The difference in gloss or matte appearance relies on the surface texture, whether it is highly smooth or it presents some roughness. Certain indoor applications require glossy paints, while for industrial and agricultural purposes, a matte paint is preferred to hide surface irregularities and damages. The gloss level of a powder coating can be reduced by the addition of a foreign compound, such as inorganic fillers or rheological additives, that can have different reactivity or curing temperature than the powder, by varying the size of the powder coating particles, by varying the humidity of the environment or by tuning the conditions during electrospraying [4–6]. Here we present a novel approach for gloss reduction that avoids the addition of foreign particles to the powder formulation, which may induce segregation or non-uniformities in the final product, but just relies on the surface modification of the primary powder coating particles to induce a transition in the surface appearance of the paint.

For that, we deposited ultrathin films of aluminium oxide (Al_2O_3) on the primary particles of a standard powder coating paint at ambient conditions by using gas-phase precursors. We evaluated how aluminium oxide films modified the flowing behaviour of the powder coating particles above the glass transition temperature, and whether that would induce roughness on the paint surface. The alumina films were deposited in a fluidized bed reactor (FBR) using a sequential exposure of precursors to the substrate, similar to the one in atomic layer deposition (ALD). A FBR allows processing large amounts of particles [7–11] while providing good mixing between gas and solids, that translates in the deposition of rather conformal alumina films. However, working

* Corresponding author.
E-mail address: J.R.vanOmmen@tudelft.nl (J. Ruud van Ommen).

http://dx.doi.org/10.1016/j.powtec.2017.05.019

at ambient conditions resulted in the deposition of thicker alumina films faster than in typical Al_2O_3 ALD processes [12,13].

ALD allows the deposition of inorganic films in a layer-by-layer growth mechanism based on two consecutive self-terminating reactions, with a purging step using an inert gas after each reaction [14,15]. The self-terminating feature of the ALD reactions ensures that the precursor molecules will only react where there is an active site available, preventing the growth of several layers of compound in each cycle [16–18]. Al_2O_3 ALD, using trimethylaluminium (TMA) and water as precursors, is commonly carried out at a range of temperatures between 33 and 170 °C and a few millibars of pressure, achieving a growth per cycle (GPC) of 0.1–0.2 nm [12,19–22]. In this work, the substrate used could not be heated to such temperatures, thus alumina films were deposited at ambient conditions, i.e. 27 ± 3 °C and 1 bar.

Working at atmospheric pressure and room temperature involves the accumulation of the unreacted precursor molecules on the surface of the substrate if they are dosed in excess above the saturation regime, inducing a chemical vapour deposition (CVD) type of reaction [23–25]. That would result inevitably in the deposition of multiple atomic layers of alumina during each cycle, depending on the amount of precursor molecules dosed to the reactor [13,26,27], producing a higher GPC than in a typical ALD process. Nevertheless, this can be beneficial to deposit thicker alumina films in a shorter time period.

Alumina ALD films have been used as passivating material, and in the production of membranes and catalysts amongst other applications [28–35]. In this work, thin Al_2O_3 films acted as physical barrier to confine the softened powder coating particles to tune the surface appearance of the cured powder coating paint. We investigated the influence of the thickness of the Al_2O_3 films on the flowability of the coated particles, and how this translated into different textures of the final paint. This experimental paper is a proof of concept for the applicability of an emerging gas-phase coating technology, such as ALD/CVD in a fluidized bed reactor, to modify the surface appearance of an industrial product, i.e. standard powder coating, while maintaining the same mechanical properties.

2. Experimental

2.1. Experimental setup and compounds

Al_2O_3 coating experiments were performed in a fluidized bed reactor similar to the one described previously [13,36], composed by a vertical glass column with a diameter of 26 mm and 500 mm in length which was located in a vertical vibration table to assist the fluidization [8]. Semiconductor grade TMA was provided by Akzo Nobel HPMO (Amersfoort, The Netherlands) in a 600 mL WW-600 stainless steel bubbler, which is kept at 30 °C during operation. Water, the second precursor, is kept in a similar bubbler, while nitrogen grade 5.0 is used as carrier and purging gas. A standard polyester powder coating paint was used as substrate. This powder coating paint is characterized by a fast and low-temperature cure, good flow and flexibility, and a gloss surface finish, ideal for architectural applications [37]. In each experiment, we coated 110 g of white standard powder coating particles provided by DSM Coating Resins (Zwolle, The Netherlands). The powder coating particles, with a Sauter mean diameter ($d_{3,2}$) of 33 μm, are composed of five components: resin, i.e. Uralac® P 3210, crosslinker, pigment, i.e. titanium oxide, flow control agent and degassing agent (more detail in [37] and *Supplementary information A*), all of them with different mass fraction in the final product. A flow of 0.4 L/min of nitrogen was used to fluidize the particles, which corresponds to a superficial gas velocity of 1.26 cm/s.

2.2. Coating experiments

The dosing times used in the coating experiments were 8–10–4–10 min for the sequence TMA–N_2–H_2O–N_2. To estimate the minimum dosing times, we used the maximum amount of aluminium atoms and methyl groups that can be allocated on the surface of a powder coating particle to obtain fully coverage. These values are 4 and 5 species per nm^2 of Al and CH_3, respectively [38,39]. The total surface area inside the column was 13 m^2 for the 110 g of powder used in each experiment, using the Sauter mean diameter of 33 μm, a particle density of 1500 kg/m^3 (*Supplementary information A*), and assuming that the particles are spherical and the calculated specific surface area of the powder is 0.12 m^2/g. The amount of precursor molecules dosed to the reactor was calculated using the vapour pressure of the precursors inside the bubblers and the ideal gas law, assuming that the TMA is a dimer at 30 °C [40,41], and that the saturation of the nitrogen bubbles inside the TMA bubbler is about 50% [42]. The theoretical dosing times to saturate the surface of the particles are respectively 0.25 and 0.24 min for TMA and water. In order to obtain thicker alumina films, we overdosed both precursors, fixing the dosing times in 8 and 4 min for TMA and water. At ambient conditions, we think that the unreacted molecules of water physisorb on the substrate surface [43–45], being involved in the following reaction with TMA molecules, also dosed in excess. The purging time of 10 min corresponds to approximately 13 times the residence time in the reactor. Using these times, we performed six coating experiments with different number of cycles, i.e. 1, 2, 3, 5, 7 and 9.

2.3. Characterization of the coated particles and sprayed panels

The influence of the alumina film thickness on the surface finish was first investigated on the individual powder coating particles. The film thickness and the growth per cycle were estimated from the mass fraction of aluminium on the samples measured by elemental analysis using ICP-OES (induced couple plasma – optical emission spectroscopy) as shown elsewhere [13]. Further, DSC (differential scanning calorimetry) was used to study whether the alumina films influenced the thermal properties of the coated particles, such as the glass transition temperature. The heat flow measured by the DSC device was normalized with the amount of powder used in each measurement, which ranged between 10 and 20 mg. Each DSC measurement consisted of a multistep program, composed by: (i) equilibration of the sample for 5 min at 25 °C, (ii) cooling from 25 to 0 °C, (iii) isothermal period of 5 min at 0 °C, (iv) heating from 0 to 130 °C, (v) isothermal period of 5 min at 130 °C, (vi) cooling from 130 to 0 °C, (vii) isothermal period of 5 min at 0 °C, (viii) heating from 0 to 170 °C, (ix) isothermal period of 10 min at 170 °C, and (x) cooling from 170 to 0 °C. All the heating and cooling steps were carried out with a rate of 10 °C/min. Steps (i), (ii) and (iii) were carried out so all the samples have the same thermal history. Steps (iv) to (vii) were carried out to have "enthalpic relaxation" of the powder, which typically occurs to amorphous resins during the glass transition [46]. Finally, steps (viii) to (x) were done to determine the glass transition temperature of the particles. With this approach, the samples were heated above the glass transition temperature during step (iv), but below the curing temperature, to prevent inducing irreversible changes on the powder coating particles. Finally, the completeness of the alumina films and its barrier performance were evaluated with a hot stage microscope and the pill flow test, which compares the flowability of the different alumina-coated powder coating particles down an inclined aluminium panel while heating the samples in an oven from room temperature to the curing temperature.

Subsequently, we sprayed the coated powders onto aluminium panels to study the influence of the alumina films on the appearance of the paints by using a corona-discharge gun and curing them in an oven at 160 °C during 10 min. The coated particles showed a poor adhesion to the panels during spraying, most likely produced by a reduction of the charge acquired by the powder while sprayed by the gun. To counteract the poor adhesion, we mixed, in a 1:1 mass ratio, the white Al_2O_3-coated powder prepared using TiO_2 as pigment with brown uncoated powder, prepared using a mixture of pigments and $BaSO_4$ as filler, in order to improve the adhesion and the contrast to facilitate

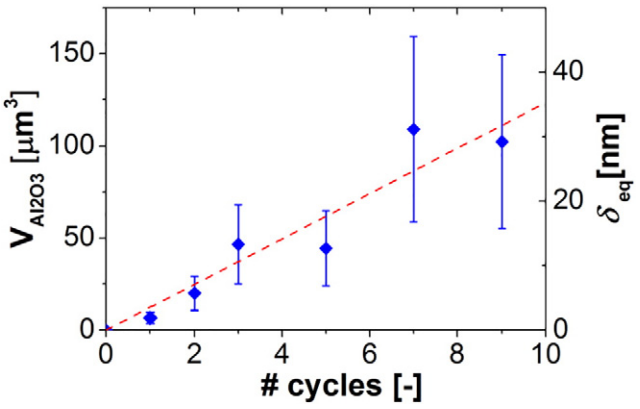

Fig. 1. Volume of aluminium oxide deposited on the particles (primary Y axis) and the equivalent film thickness (secondary Y axis) were calculated assuming spherical particles, and uniform and complete alumina films. The increase of the film thickness can be approximated with a linear trend, where the slope represents a GPC of 3.5 nm. The error bars represent the uncertainty in the calculation of the film thickness.

the characterization of the painted panels. The other components of both powders, i.e., the additives, are the same.

The surface topography of the painted panels was studied by visual observation, and a SEM (scanning electron microscope) coupled with EDX (energy dispersive X-ray) analysis was used to have a closer look at the surface of the panels. In addition, the roughness of the panels was measured with surface profilometry and the gloss of the paints with a haze-gloss meter. Finally, the mechanical resistance was evaluated upon the impact of a steel ball in the reverse side of the panels. More details of the characterization techniques are given in *Supplementary information B.*

3. Results and discussion

3.1. Characterization of the coated particles

We performed six coating experiments, with different number of cycles, on white powder coating particles, and estimated the film thickness using the fraction of aluminium obtained from elemental analysis with ICP-OES. The uncoated white powder coating particles contained a mass fraction of aluminium of 0.0064, coming from the TiO_2 (*Supplementary information C*). The volume of aluminium oxide ($V_{Al_2O_3}$) is calculated from the fraction of aluminium on the coated samples, using a density of alumina of 2500 kg/m^3 [21]. From this value, an equivalent film thickness of alumina (δ_{eq}) is calculated assuming that the particles are spherical and coated uniformly. We refer to this value as "equivalent film thickness" since the coating process requires a certain number of cycles to form a complete alumina film [39,47], that is, there is not yet a complete film after few coating cycles, since the precursor molecules penetrate the polymeric matrix during those cycles. The content of aluminium on the coated samples (i.e., in the deposited volume of aluminium oxide) increased with an increasing number of cycles; see Fig. 1. The GPC is calculated from the slope of the linear fit shown by the red-dotted line. The uncertainty in the calculation of the film thickness is represented by the error bars in Fig. 1 (more details can be found in *Supplementary Information C*). We obtained a GPC of 3.5 nm, much larger than the typically values for Al_2O_3 ALD, i.e. 0.1–0.2 nm. This is explained by the accumulation of the overdosed precursor molecules at ambient conditions, which would react in the subsequent reaction. The increase in the experimental dosing time of TMA, 8 min, compared to the theoretical one, 0.25 min, is comparable to the values of the GPC, which increased from 0.15 nm in a standard ALD process to 3.5 nm in our process. Obtaining such high GPC benefited our process, since we were able to deposit thick alumina films faster, although this process can no longer be referred to as atomic layer deposition.

We studied whether the aluminium oxide films act as an insulating layer, changing the thermal properties of the powder, or only as a physical barrier, preventing the softened powder from flowing freely. The glass transition temperature of the powder (T_g) was measured with DSC, and a hot stage microscope was used to observe the particles above the T_g. The results from both techniques were combined to identify the influence of the alumina films on the powder coating particles.

The DSC measurements in Fig. 2 show the heating phase, with positive normalized heat flows, and the cooling phase, with negative normalized heat flows. During the heating, the glass transition is observed as the step function at around 50 °C. The powder coating is amorphous, so we refer to it as *softening* of the particles above the glass transition. Fig. 2 only shows steps (viii), (ix) and (x) of the measurements (see Experimental section). The full DSC profile is given in *Supplementary information D.*

First, the DSC profile of a powder that was fluidized during 3 h at the coating temperature, i.e. 27 °C, was measured and compared with the profile of the unprocessed powder (Fig. 2a). Both uncoated and fluidized samples have the same glass transition temperature and heat flow profiles, indicating that the fluidization process did not alter the thermal properties of the powder. Fig. 2b shows the normalized heat flow profiles for the uncoated and coated samples. The curves of all the samples show the step function at the same temperature, meaning that the glass transition is not affected by the alumina films. Therefore, it can be concluded that the alumina films did not act as thermal insulator for the powder, since the glass transition of all the samples occurred at the same temperature. Then, we investigated the effect of the alumina films as a physical barrier.

A hot stage mounted on a light microscope was used to determine the confinement efficiency of the alumina films by observing whether the softened powder, above its glass transition temperature, would flow freely or remain enclosed. For that, few particles were placed on a quartz plate, which was placed on top the hot stage, and all together on the microscope stage. The samples were heated from 25 to 70 °C with a heating rate of 10 °C/min, similar to the one used in the DSC measurements. Fig. 3 shows the micrographs of the uncoated, 1-cycle, 2-cycle, 3-cycle and 9-cycle samples.

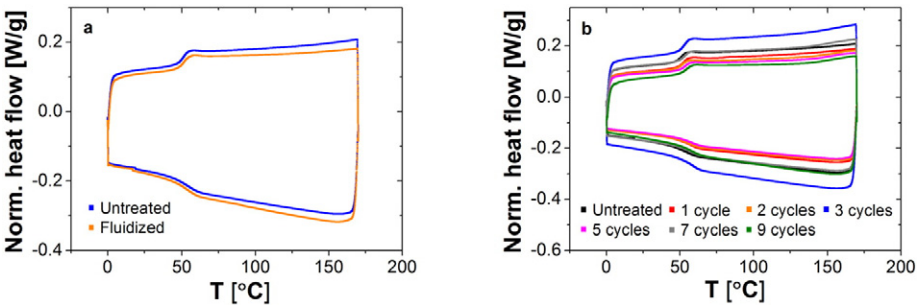

Fig. 2. (a) DSC profiles of the untreated and fluidized powder. (b) DSC profiles of the powder of the untreated sample and the samples coated with 1, 2, 3, 5, 7 and 9 cycles.

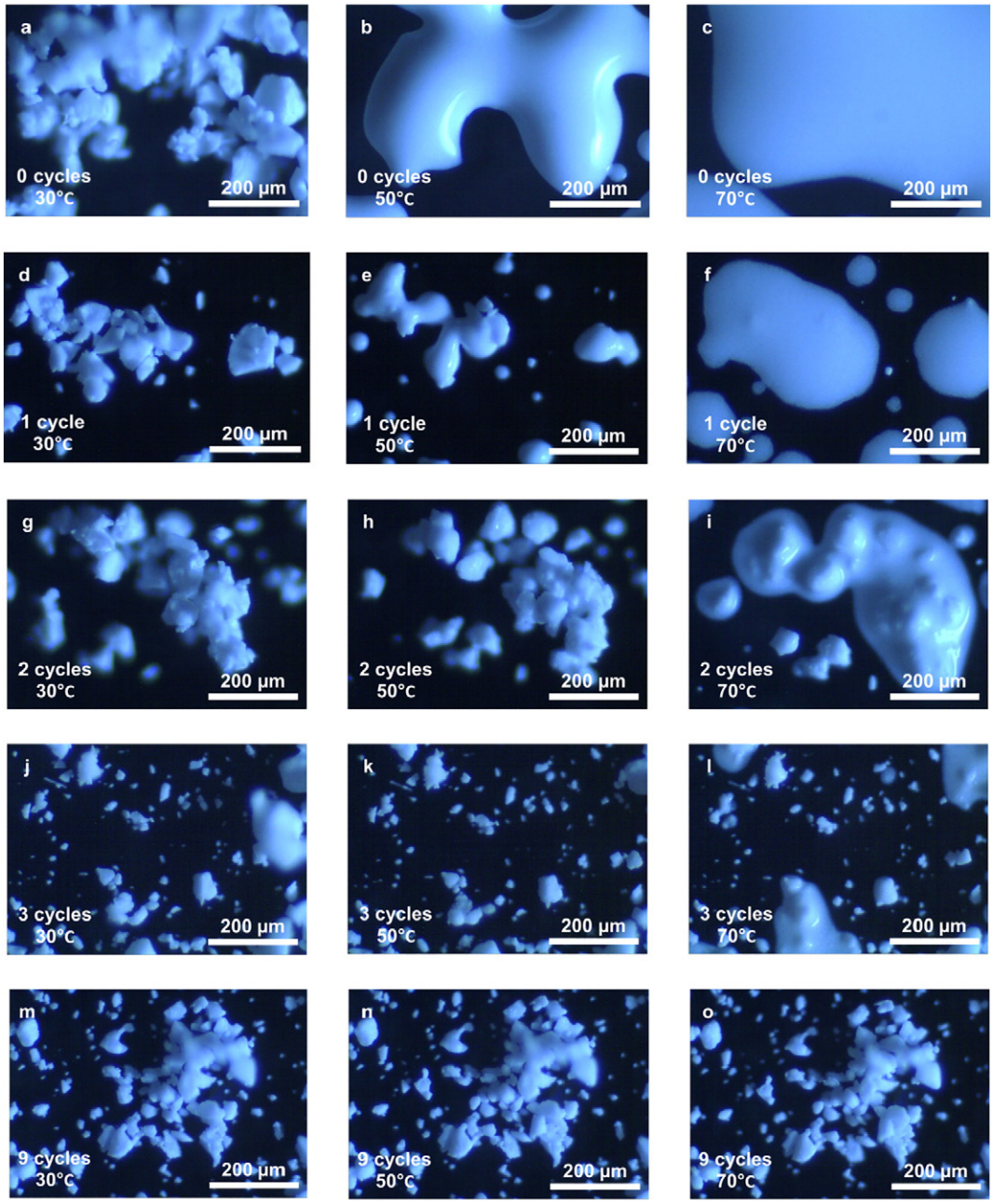

Fig. 3. Hot stage microscope images of the uncoated powder (a–c) and the samples coated with 1 (d–f), 2 (g–i), 3 (j–l) and 9 (m–o) cycles, at 30, 50 and 70 °C.

The softening of the uncoated particles (Fig. 3a-c) started at about 45 °C, slightly lower than the 50 °C observed in the DSC curves. In the hot stage microscope, there were losses of heat to the surrounding air since the sample is in contact with the environment, while in DSC the samples are placed inside an isothermal chamber. That could cause the difference in the measured softening temperatures in the DSC and the hot stage microscope. The hot stage microscope was used to compare all the samples, which would experience the same heating process using the same equipment. In order to have a better view of the particles, the samples were illuminated with a LED light source. This provided a 3D-like visualization of the particles if compared with the micrographs that were taken using the built-in light of the microscope (*Supplementary information E*). The bluish colour seen in Fig. 3 is produced by the LED light source.

The uncoated (Fig. 3a-c) and 1-cycle (Fig. 3d-f) powders softened and flowed at about the same temperature. However, a fraction of the sample coated with 2 cycles (Fig. 3g-i) remained enclosed within the alumina film, similar to what was observed with the 3-cycle sample (Fig. 3j-l). The particles of the sample coated with 7 and 9 cycles preserved their shape, indicating that the alumina coating was able to enclose the softened powder coating paint (Fig. 3m-o and *Supporting Information E*). This proves that the powder coating particles coated with 7 or more cycles created core-shell structures. Micrographs of

Table 1
Values used in the calculation of the tensile stress $\sigma_c^{Al_2O_3}$.

Variable	α_V	αL	β	E	υ
Units	[1/°C]	[1/°C]	1/MPa	GPa	–
Value	$100 \cdot 10^{-6}$	$5 \cdot 10^{-6}$	$9.2 \cdot 10^{-4}$	170	0.24
Reference	[52]	[54]	[53]	[55]	[55]

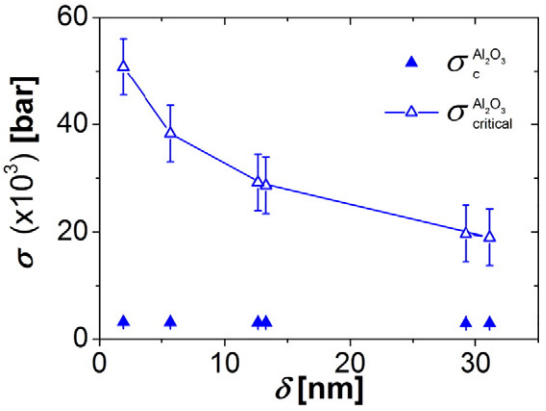

Fig. 4. Tensile stress ($\sigma_c^{Al_2O_3}$) exerted on the alumina-coated samples (blue symbols) and critical tensile stress ($\sigma_{critical}^{Al_2O_3}$) of the alumina before breaking (open symbols) for the different film thickness. The error bars represent the uncertainty in the calculation of the tensile stresses.

the samples using the light source in transmission mode of the microscope were also taken to count the fraction of the particles that remained contained above the glass transition temperature (*Supplementary information E*). About 130 particles per sample were observed to determine the percentage of the particles that remained encapsulated. All the particles of the uncoated and 1-cycle samples flowed out once softened, and eventually coalesced. About 5% for the 2-cycle sample, 41% for the 3-cycle sample, and 62% for the 5-cycle sample remained enclosed by the alumina films. For higher number of cycles, that is, 7 and 9 cycles, all the particles remained completely encapsulated, observing no deformation in any of the particles. The combination of the results from DSC, which showed that the glass transition temperature is not altered by the alumina films, and the one from the hot stage microscope, which showed that there is a key number of cycles above which the particles remained encapsulated, we conclude that the alumina films do not act as a thermal insulating layer, but as a physical barrier.

These results suggest that there is a critical number of cycles above which the alumina film is sufficiently thick and completely closed to contain the softened particles (Fig. 3o). We propose two hypotheses: (i) the alumina films are free of defects, and the stress caused inside the shell by expansion upon softening is higher than the stress that the deposited alumina shell can endure, resulting in the release of the softened core; and (ii) that a certain number of coating cycles are required to form a complete alumina film, based on the nucleation of the alumina ALD during the initial cycles when using polymeric particles as substrate [47,48].

To calculate the resistance of the alumina films upon an increase of the internal pressure p (Eq. (1)), we modelled the core-shell particles as a "thin-walled spherical vessel" [49]. This model can only be used when the ratio of the film thickness to particle diameter is smaller than 0.1, which is the case for our particles. By using this approach, we can calculate the tensile stress on the alumina coating ($\sigma_c^{Al_2O_3}$) caused by the expansion of the core (Eq. (2)), and compare it to the critical tensile stress before cracks appear in the alumina coating ($\sigma_{critical}^{Al_2O_3}$), calculated using (Eq. (3)). A detailed explanation of these calculations can be found in *Supplementary information F*.

$$p = \frac{(\alpha_V - 3\cdot\alpha_L)\cdot\Delta T}{\frac{3}{4}\cdot\frac{d_{3,2}}{E\cdot\delta}\cdot(1-\upsilon)+\beta} \quad (1)$$

$$\sigma_c^{Al_2O_3} = \frac{p\cdot d_{3,2}}{4\cdot\delta} \quad (2)$$

$$\sigma_{critical}^{Al_2O_3} = E\cdot\varepsilon_{critical} \quad (3)$$

Here, $d_{3,2}$ is the Sauter mean diameter of the particles, α_v is the volumetric coefficient of thermal expansion of the core material, α_L is the linear coefficient of thermal expansion of the alumina shell [54], ΔT is the difference in temperature between the final T_f and initial T_i state, i.e. 70 and 25 °C, E and υ are the Young modulus and Poisson's ratio of pure aluminium oxide films deposited by ALD [55], β is the compressibility factor of the core material (Table 1), δ is the alumina film thickness and $\varepsilon_{critical}$ is the critical strain of alumina films deposited by ALD under a tensile stress, which depends on the film thickness [50,51]. The values of the coefficient of thermal expansion α_V and the compressibility factor β were taken from literature for a similar resin [52,53], since we could not determine these two parameters for our material with a good accuracy. Despite that, a sensitivity analysis of these two variables, α_V and β indicated that they do not have a strong impact on the value of $\sigma_c^{Al_2O_3}$. The values of the equivalent film thickness (Fig. 1) were used to calculate both tensile stresses ($\sigma_c^{Al_2O_3}$ and $\sigma_{critical}^{Al_2O_3}$).

The results in Fig. 4 indicates that the aluminium oxide films deposited in these coating experiments would break under a much larger tensile stress ($\sigma_{critical}^{Al_2O_3}$) than the one produced by the expansion of the softened resin ($\sigma_c^{Al_2O_3}$). The model predicts that the alumina films would resist the internal pressure in all the cases, while experimental evidences show that the softened powder flowed out the alumina shell for the samples with less than 7 coating cycles. We used the values for E and υ of pure alumina films deposited by ALD, which may differ from the ones of the alumina films deposited at ambient conditions. However, the difference between the calculated values of the critical and tensile strength is very large, thus, we think there is not a strong influence of these alumina properties on the calculation. Based on modelling results of Fig. 4, we conclude that the onset of flowing is not caused by breaking of the shell. Rather, samples with a small number of cycles start flowing because a closed film has not formed yet, allowing the resin to escape as soon as it softens.

This analysis agrees with the nucleation theory of alumina ALD on polymeric substrates [47,48]. During the first coating cycles, precursor molecules penetrate through the polymer surface to deposit as alumina nuclei (Fig. 5). This is promoted by factors such as the solubility of TMA on hydrophobic surfaces, the rough surface of the resin particles, and the free volume near the surface of these materials due to the lack of lattice structure and crystallinity, which is seen as a porosity that can be accessed by the precursors. Although the nucleation phenomenon is qualitatively understood, there is no rule-of-thumb for the number of cycles needed to deposit fully conformal films, since this depends on the polymer nature, preparation method, polymer history, etc. Based

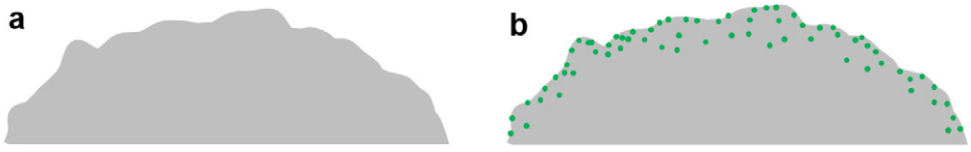

Fig. 5. Nucleation mechanism of the deposited alumina. (a) Surface of the untreated polymer particle. (b) Surface of the polymer particle during the first cycles, in which the green spheres represent the alumina molecules.

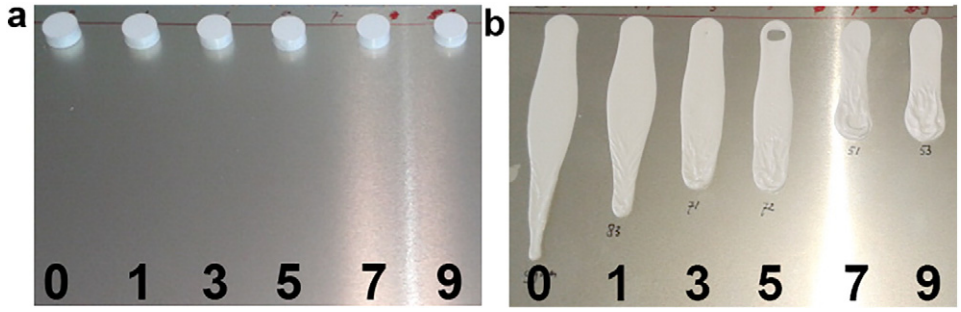

Fig. 6. Pill Flow test panel before (a) and after (b) introducing it in the oven at 160 °C for 10 min, which is the curing procedure for this powder. The pills correspond, from left to right, to the 0, 1, 3, 5, 7 and 9-cycle samples. The pills have a diameter of about 10 mm, and 5 mm height.

on the hot stage microscopy analysis, it appears that after 7 coating cycles a conformal and complete aluminium oxide film was deposited on the particles, creating a core-shell structure (Fig. 3 and *Supplementary information E and F*).

The degree of confinement of the coated particles was also studied with the pill flow test, which analyses the flowability of a pill prepared with the powder coated with alumina (Fig. 6a) down an inclined panel upon heating between room temperature and the curing temperature of the paint. Fig. 6b shows a reduction of the length of the trail even after 1 alumina coating cycle compared to the uncoated sample. This length kept decreasing when increasing the number of cycles. Interestingly, the sample coated with 9 cycles showed a displacement down the inclined panel, while it remained totally encapsulated in the hot stage microscope (Fig. 3m-o). To prepare the pills a pressure of 5000 psi is applied to compact the powder; it is possible that part of the alumina film broke because of the compression, creating a way out for the softened core and letting it flow down the panel. The results from the pill flow test are in agreement with the DSC and hot stage microscopy, which prove that the alumina film acts as a physical barrier preventing the softened particles from flowing freely. We further investigated the impact of the alumina films on the appearance of the final product, the powder coating paint.

3.2. Characterization of the sprayed panels

In total, seven panels were sprayed with the 1:1 mass ratio mixtures of the uncoated brown and coated white particles, i.e., the powder with 0, 1, 2, 3, 5, 7 and 9 cycles. Visual inspection of the panels (Fig. 7a) indicated a transition in the surface appearance of the panels, regarding both colour and roughness, for the powder coated with more than 2 cycles. The panels prepared with the uncoated white powder and the 1-cycle powder (Fig. 7a, ⓪ and ①) showed a predominant white colour, while a brown colour dominated the panels prepared with the 2-, 3-, 5-, 7- and 9-cycle samples (Fig. 7a, ②, ③, ⑤, ⑦ and ⑨). The reduction of the gloss of the paints, caused by the surface roughness, was visualized by illuminating the panels with LED light sources in a dark environment (Fig. 7b and c). The surface of the panels ⓪ and ① is smooth, producing reflection of the light on the panels. Increasing the number of cycles induced roughness of the surface, producing a diffused reflection of the LED lights on the ②, ③, ⑤, ⑦ and ⑨ panels.

The measurements of the surface roughness (Fig. 8a) and the gloss of the coatings (Fig. 8b) indicated that the rougher the surface is, the more light it scatters, resulting in a less glossy paint. The surface roughness increased with the number of cycles, reaching a constant value of about 9 μm after 7 cycles, which corresponds to 1/3 of the particle size. A similar trend was observed for the values of the gloss, which significantly dropped for 2 or more cycles, in agreement with the observation of the surface roughness. A gloss level above 60 gloss units (GU) correspond to a glossy surface, while below 35 GU the surface is considered to have a matte finish, according to the internal standards of DSM Powder Coating Resins. During the curing step, the brown powder softened above the glass transition temperature forming a continuous layer, while the alumina coated white powder, which flowed out of the alumina shell (depending on the number of coating cycles), would be suspended on the brown softened layer, inducing the roughness. Both surface roughness and gloss measurements agree with other results in which the alumina film after 2 cycles altered already the flowing behaviour of the single particles.

An optical microscope (Fig. 9) and a SEM equipped with EDX detector (Figs. 10 and 11) were used to take a closer look at the surface of the panels and study the transition in the surface appearance, i.e., the colour and roughness. The optical microscope showed different distributions of the cured white and brown powder coated paint for the samples prepared with 1 and 3 alumina-coated particles. The panels sprayed with uncoated (Fig. 9a) and 1-cycle (Fig. 9b) white powder coating particles exhibited an homogeneous distribution of the brown and white colours, explained by the good flow of both white and brown particles (Fig. 3c and f). The panel prepared with the 3-cycle sample (Fig. 9c) showed a less uniform distribution of the colours, caused by the partial

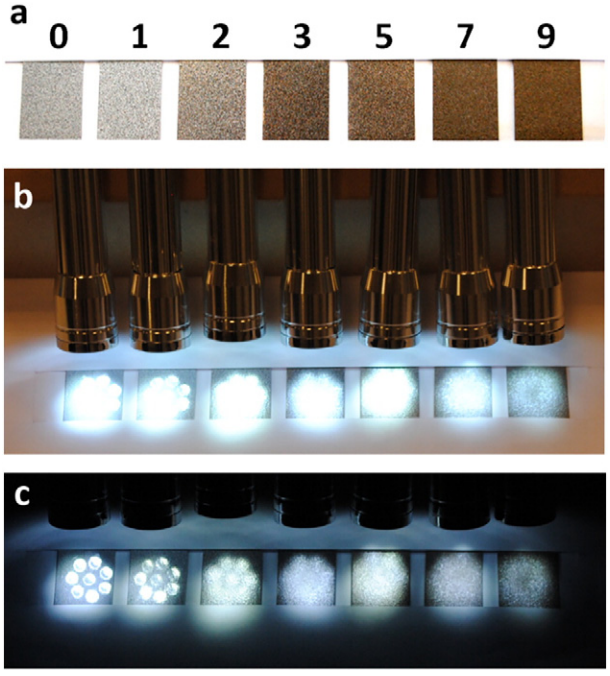

Fig. 7. (a) Piece of the sprayed panels after curing at 160 °C for 10 min, prepared with the mixture of white powder coated with 0, 1, 2, 3, 5, 7 and 9 cycles, and uncoated brown powder coating paint (from left to right). The dimensions of the panels shown are 22 × 25 mm. The same panels were illuminated with LED lights in a light environment (b) and dark environment (c) to show the gradual decrease in the gloss level of the panels with the number of coating cycles.

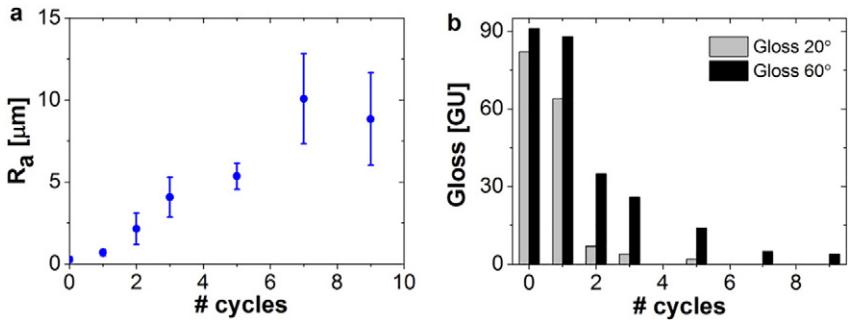

Fig. 8. (a) Measurement of the roughness of the panels sprayed with a 1:1 mixture of white alumina-coated and brown uncoated powder coating. The roughness was measured with a surface profilometer. Error bars represent the standard deviation of the measurements. (b) Glossiness of the panels was measured with a gloss meter at 20° and 60°.

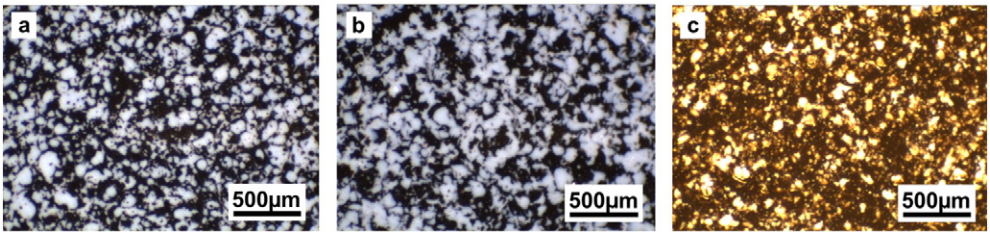

Fig. 9. Images from the optical microscope. Panels sprayed with (a) uncoated powder, (b) 1-cycle coated powder, and (c) 3-cycle coated powder.

confinement of the white powder and the consequent decrease of the mixing between the white and brown powders after softening. To evaluate this panel (Fig. 9c), the incident angle and intensity of the light source was modified to overcome the reflection on the panel caused by the roughness, creating a yellowish colour. In Fig. 9a and b, both white and brown particles softened, flowed and mixed homogeneously, creating a uniform pattern. Fig. 9c suggests that while the brown powder softened, the white powder only did to a lesser extent, creating a kind of suspension of white grains in a brown uniform matrix.

The roughness formation on the panels was investigated with a SEM microscope (Fig. 10) equipped with EDX detector (Fig. 11). Two different SEM modes were used to look at the surface: Back-scattering Topology BET, (Fig. 10a, c and e), and Back-scattering Composition BEC, (Fig. 10b, d and f). The panels sprayed with the uncoated particles (Fig. 10a) did not show roughness in the topology mode, in agreement with the visual observation (Fig. 7). Nevertheless, the composition-mode picture revealed darker and brighter areas (Fig. 10b). As we expected, BET-mode images of the 3-cycle (Fig. 10c) and the 9-cycle (Fig. 10e) panels confirmed the presence of surface roughness, which corresponded to the darker areas observed in the analogous BEC-mode pictures (Fig. 10d and f). The composition of the darker and brighter areas in the BEC-mode images and its relation with the roughness in the BET-mode images was examined with EDX.

Full area EDX and spot EDX analysis were performed on both brighter (①) and darker (②) areas of the samples (Fig. 11). The brighter areas (white bars in Fig. 11) were composed of higher concentrations of Barium (Ba) and Sulphur (S), while the darker areas (black bars in Fig. 11) had a dominant concentration of Titanium (Ti). This corresponds to the presence of $BaSO_4$, which is the filler used in brown powder coatings, and TiO_2 used as pigment in the preparation

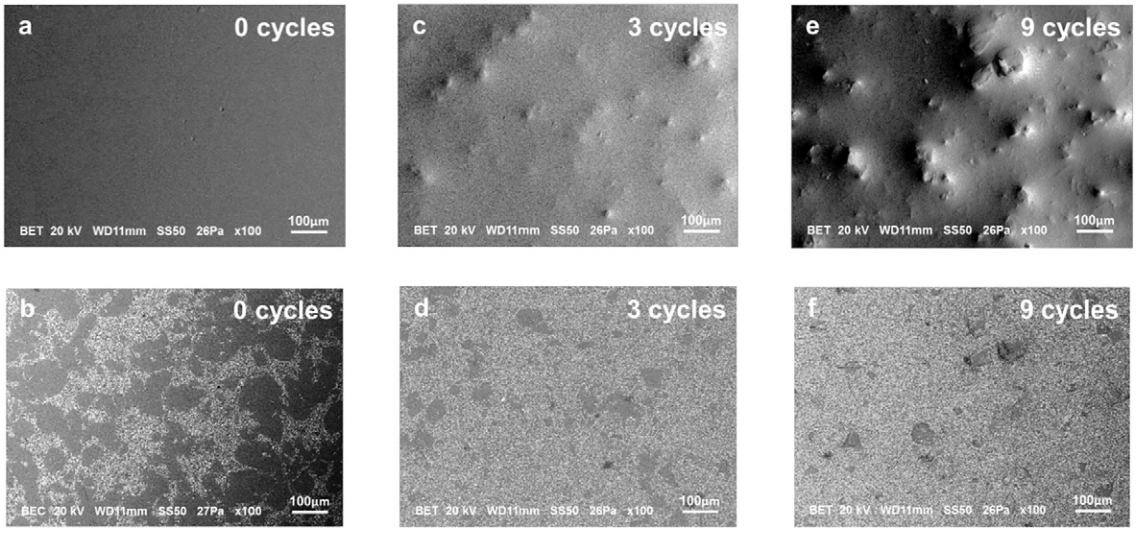

Fig. 10. SEM pictures using topology mode (BET) (a, c, e) and composition mode (BEC) (b, d, f) of the panels prepared with uncoated particles (a) and (b), 3-cycle particles (c) and (d), and 9-cycle particles (e) and (f). The duplet of pictures for each sample represent the same area of the panel.

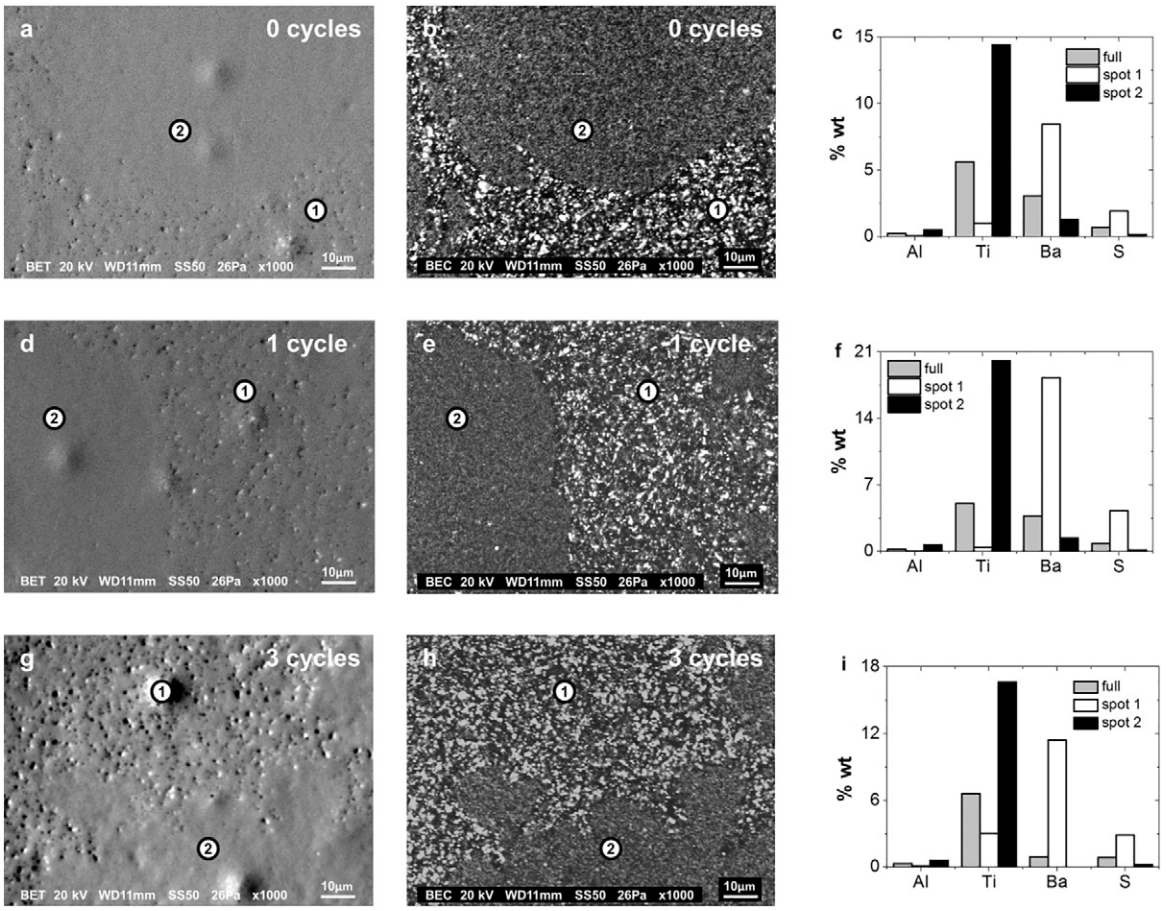

Fig. 11. SEM images using the topology mode (BET) for the samples sprayed with 0 cycles (a), 1 cycles (d) and 3 cycles (g), and the composition mode (BEC) mode for the samples with 0 cycles (b), 1 cycles (e) and 3 cycles (h). Pictures (c), (f) and (i) show the EDX analysis of the full image (grey bars), spot 1 (white bars) and spot 2 (black bars).

of the white powder. Higher concentrations of aluminium were found in the darker areas, which correspond to the Al_2O_3-coated white powder coating. Other compounds identified by EDX analysis, such as C, O and N, are not included in Fig. 11 since they were detected in all the panels. The combination of the SEM (Fig. 10), which related the presence of darker and brighter areas with the roughness of the surface, and the EDX analysis (Fig. 11), which pointed out the presence of white pigment and aluminium in the darker areas, prove that the increased roughness and consequent reduction in the gloss level of the paints were caused by the Al_2O_3-coated particles.

To conclude, the mechanical resistance of the sprayed paints was evaluated with the *reverse impact test* (*Supplementary information G*). This test studies the formation of cracks on the panels as the result of the impact of a steel ball released from a certain height. In this work,

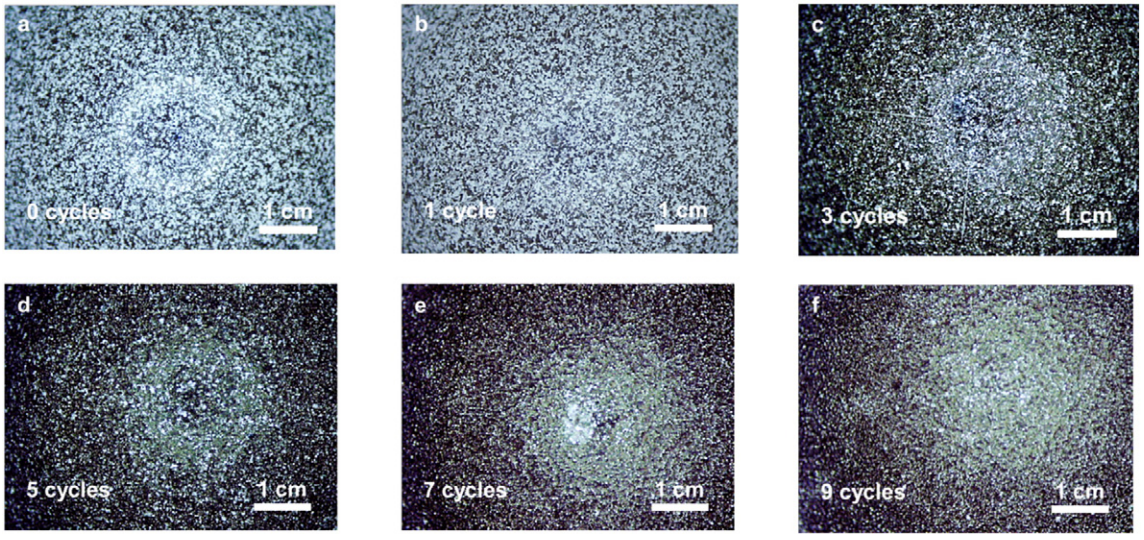

Fig. 12. Reverse Impact test, performed over the painted panels with 0, 1, 3, 5, 7 and 9 cycles. The thickness of the paint was around 50 μm in all the samples. The contrast and brightness of the pictures were modified for a better visualization of the cracks.

we used a stereomicroscope to observe the footprint of the impact of the ball on the surface of the panel (Fig. 12). The contrast and brightness of the pictures in Fig. 12 were tuned to improve the visualization of impact on the panels. The impact of the ball deformed the panels, as seen in the centre of the images, in which the cracks would appear. We found that all the panels showed good impact resistance.

From the results obtained, we conclude that powder coating particles coated with only 2 cycles of alumina induced a granular textured paint, characterized by a rough and matte surface finish with good impact resistance. Nevertheless, this process can be further optimized. For instance, the dosing and purging times, in combination with the number of cycles, would lead to a more time-efficient coating process. Likewise, variables such as the particle size and the ratio of the coated-to-uncoated powder mixtures influence the appearance, i.e. roughness, gloss and colour, and the mechanical resistance of the paint. This work did not aim at obtaining an industrial solution for the production of a matte powder coating paint, but at proving the applicability of gas-phase coating techniques on particles, such as ALD or CVD, to modify and improve the properties of industrial products. In this work, roughness was induced while maintaining good mechanical properties on a glossy DSM Powder Coating Resin containing standard powder coating paint.

4. Conclusions

We showed that a thin aluminium oxide film deposited on particles of a standard dry powder coating paint delayed or even completely suppressed the fluid-like behaviour above the glass transition temperature. As a result, the appearance of the final paint could be tuned between a gloss finish and a matte one, depending on the number of alumina coating cycles on the paint particles. The coating process was carried out in a fluidized bed reactor operated at 27 °C and 1 bar, using trimethylaluminium and water as precursors. The precursors were fed in subsequent steps, similarly to ALD. However, operating at ambient conditions combined with a dosing of both precursors in excess resulted in a growth of about 3.5 nm of Al_2O_3 per cycle, much higher than in typical ALD processes. We found that after 2 coating cycles, the alumina deposited was sufficient to alter the flow of the particles and the appearance of the paint. More cycles resulted in thicker alumina coatings that further modified the paint appearance, whereas more than 5 cycles had little additional effect. The suppression of flow was not caused by delayed softening due to thermal insulation by the alumina films, as determined by differential scanning calorimetry. Rather, the films acted as a hard physical shell that prevents material release from the core that softens irrespective of the coating around it. The thickness of the film is not important as long as it covers the entire particle. We calculated that the thinnest shell is strong enough to contain the core, even when the core softens and expands due to heating, using an order-of-magnitude analysis in a thin-wall spherical-vessel model. We found, after interpretation of the results from SEM and EDX, that Al_2O_3 can readily alter the flowing behaviour and induce roughness in paints, while keeping the mechanical resistance comparable to the reference paints.

Acknowledgments

The research leading to these results has received funding from the European Union Seventh Framework Program FP7/2007–2013 under grant agreement no. 264722. The authors acknowledge to Royal DSM for partly funding this research.

Appendix A. Supplementary data

Supplementary data to this article can be found online at http://dx.doi.org/10.1016/j.powtec.2017.05.019.

References

[1] J. Verlaak, Broader scope for powder coatings: resin developments benefit applicators, end users and the environment, Eur. Coat. J. 12 (2009) 86–89.
[2] T.A. Misev, R. van der Linde, Powder coatings technology: new developments at the turn of the century, Prog. Org. Coat. 34 (1–4) (1998) 160–168.
[3] E. Spyrou, Powder Coatings Chemistry and Technology, Vincentz Network, 2013.
[4] S.S. Lee, J.H. Koo, S.G. Chai, J.C. Lim, Gloss reduction in low temperature curable hybrid powder coatings, Prog. Org. Coat. 46 (4) (2003) 266–272.
[5] W. Jacobs, D. Foster, S. Sansur, R.G. Lees, Durable glossy, matte and wrinkle finish powder coatings crosslinked with tetramethoxymethyl glycoluril, Prog. Org. Coat. 29 (1–4) (1996) 127–138.
[6] A.S. Biris, M.K. Mazumder, C.U. Yurteri, R.A. Sims, J. Snodgrass, S. De, Gloss and texture control of powder coated films, Part. Sci. Technol. 19 (3) (2001) 199–217.
[7] D. Kunii, O. Levenspiel, Fluidization Engineering, second ed. Butterworth-Heinemann, 1991.
[8] J.R. van Ommen, J.M. Valverde, R. Pfeffer, Fluidization of nanopowders: a review, J. Nanopart. Res. 14 (3) (2012) 1–29.
[9] L.F. Hakim, J. Blackson, S.M. George, A.W. Weimer, Nanocoating individual silica nanoparticles by atomic layer deposition in a fluidized bed reactor, Chem. Vap. Depos. 11 (10) (2005) 420–425.
[10] A. Goulas, J.R. van Ommen, Scalable production of nanostructured particles using atomic layer deposition, Kona Powder Part. J. 31 (1) (2014) 234–246.
[11] D. Longrie, D. Deduytsche, C. Detavernier, Reactor concepts for atomic layer deposition on agitated particles: a review, J. Vac. Sci. Technol. A 32 (1) (2014) (-).
[12] J.D. Ferguson, A.W. Weimer, S.M. George, Atomic layer deposition of ultrathin and conformal Al_2O_3 films on BN particles, Thin Solid Films 371 (1) (2000) 95–104.
[13] D. Valdesueiro, G. Meesters, M. Kreutzer, J. van Ommen, Gas-phase deposition of ultrathin aluminium oxide films on nanoparticles at ambient conditions, Materials 8 (3) (2015) 1249–1263.
[14] G.V. Sveshnikova, S.I. Kol'Tsov, V.B. Aleskovskii, Formation of a silica layer of predetermined thickness on silicon by the molecular-layering method, Zh. Prikl. Khim. 43 (5) (1970) 1150–1152.
[15] T. Suntola, Atomic layer epitaxy, Mater. Sci. Rep. 4 (5) (1989) 261–312.
[16] S.M. George, Atomic layer deposition: an overview, Chem. Rev. 110 (1) (2010) 111–131.
[17] V. Miikkulainen, M. Leskelä, M. Ritala, R.L. Puurunen, Crystallinity of inorganic films grown by atomic layer deposition: overview and general trends, J. Appl. Phys. 113 (2) (2013) 1–101.
[18] D.M. King, X. Liang, A.W. Weimer, Functionalization of fine particles using atomic and molecular layer deposition, Powder Technol. 221 (2012) 13–25.
[19] L.F. Hakim, S.M. George, A.W. Weimer, Conformal nanocoating of zirconia nanoparticles by atomic layer deposition in a fluidized bed reactor, Nanotechnology 16 (7) (2005) S375–S381.
[20] J.R. Wank, S.M. George, A.W. Weimer, Nanocoating individual cohesive boron nitride particles in a fluidized bed by ALD, Powder Technol. 142 (1) (2004) 59–69.
[21] M.D. Groner, F.H. Fabreguette, J.W. Elam, S.M. George, Low-temperature Al_2O_3 atomic layer deposition, Chem. Mater. 16 (4) (2004) 639–645.
[22] M. Knez, A. Kadri, C. Wege, U. Gösele, H. Jeske, K. Nielsch, Atomic layer deposition on biological macromolecules: metal oxide coating of tobacco mosaic virus and ferritin, Nano Lett. 6 (6) (2006) 1172–1177.
[23] H.B. Profijt, S.E. Potts, M.C.M. Van De Sanden, W.M.M. Kessels, Plasma-assisted atomic layer deposition: basics, opportunities, and challenges, J. Vac. Sci. Technol. A 29 (5) (2011).
[24] S.E. Potts, W.M.M. Kessels, Energy-enhanced atomic layer deposition for more process and precursor versatility, Coord. Chem. Rev. 257 (23–24) (2013) 3254–3270.
[25] D.J.H. Emslie, P. Chadha, J.S. Price, Metal ALD and pulsed CVD: fundamental reactions and links with solution chemistry, Coord. Chem. Rev. 257 (23–24) (2013) 3282–3296.
[26] D. Valdesueiro, P. Garcia-Triñanes, G.M.H. Meesters, M.T. Kreutzer, J. Gargiuli, T.W. Leadbeater, D.J. Parker, J.P.K. Seville, J.R. Van Ommen, Enhancing the activation of silicon carbide tracer particles for PEPT applications using gas-phase deposition of alumina at room temperature and atmospheric pressure, Nucl. Instrum. Methods Phys. Res., Sect. A 807 (2016) 108–113.
[27] D. Valdesueiro, M.K. Prabhu, C. Guerra-Nunez, C.S.S. Sandeep, S. Kinge, L.D.A. Siebbeles, L.C.P.M. de Smet, G.M.H. Meesters, M.T. Kreutzer, A.J. Houtepen, J.R. van Ommen, Deposition mechanism of aluminum oxide on quantum dot films at atmospheric pressure and room temperature, J. Phys. Chem. C 120 (8) (2016) 4266–4275.
[28] B. Moghtaderi, I. Shames, E. Doroodchi, Combustion prevention of iron powders by a novel coating method, Chem. Eng. Technol. 29 (1) (2006) 97–103.
[29] L.F. Hakim, C.L. Vaughn, H.J. Dunsheath, C.S. Carney, X. Liang, P. Li, A.W. Weimer, Synthesis of oxidation-resistant metal nanoparticles via atomic layer deposition, Nanotechnology 18 (34) (2007).
[30] D.M. King, X. Liang, B.B. Burton, M. Kamal Akhtar, A.W. Weimer, Passivation of pigment-grade TiO_2 particles by nanothick atomic layer deposited SiO_2 films, Nanotechnology 19 (25) (2008).
[31] X. Liang, D.M. King, M.D. Groner, J.H. Blackson, J.D. Harris, S.M. George, A.W. Weimer, Barrier properties of polymer/alumina nanocomposite membranes fabricated by atomic layer deposition, J. Membr. Sci. 322 (1) (2008) 105–112.
[32] X. Liang, A.D. Lynn, D.M. King, S.J. Bryant, A.W. Weimer, Biocompatible interface films deposited within porous polymers by atomic layer deposition (ALD), ACS Appl. Mater. Interfaces 1 (9) (2009) 1988–1995.
[33] P. Lichty, X. Liang, C. Muhich, B. Evanko, C. Bingham, A.W. Weimer, Atomic layer deposited thin film metal oxides for fuel production in a solar cavity reactor, Int. J. Hydrog. Energy 37 (22) (2012) 16888–16894.

[34] P. Lichty, M. Wirz, P. Kreider, O. Kilbury, D. Dinair, D. King, A. Steinfeld, A.W. Weimer, Surface modification of graphite particles coated by atomic layer deposition and advances in ceramic composites, Int. J. Appl. Ceram. Technol. 10 (2) (2013) 257–265.
[35] S.P. Sree, J. Dendooven, T.I. Koranyi, G. Vanbutsele, K. Houthoofd, D. Deduytsche, C. Detavernier, J.A. Martens, Aluminium atomic layer deposition applied to mesoporous zeolites for acid catalytic activity enhancement, Catal. Sci. Technol. 1 (2) (2011) 218–221.
[36] R. Beetstra, U. Lafont, J. Nijenhuis, E.M. Kelder, J.R. Van Ommen, Atmospheric pressure process for coating particles using atomic layer deposition, Chem. Vap. Depos. 15 (7–9) (2009) 227–233.
[37] D.S.M. Powder Coating Resins, DSM Uralac P 3210 technical data sheet(accessed on 2016 May 31) www.dsmcoatingresins.com.
[38] R.L. Puurunen, Correlation between the growth-per-cycle and the surface hydroxyl group concentration in the atomic layer deposition of aluminum oxide from trimethylaluminum and water, Appl. Surf. Sci. 245 (1–4) (2005) 6–10.
[39] R.L. Puurunen, Growth per cycle in atomic layer deposition: a theoretical model, Chem. Vap. Depos. 9 (5) (2003) 249–257.
[40] A.W. Laubengayer, W.F. Gilliam, The alkyls of the third group elements. I. Vapor phase studies of the alkyls of aluminum, gallium and Indium1, J. Am. Chem. Soc. 63 (2) (1941) 477–479.
[41] C.H. Henrickson, D.P. Eyman, Lewis acidity of alanes. Interactions of trimethylalane with sulfides, Inorg. Chem. 6 (8) (1967) 1461–1465.
[42] B. Mayer, C.C. Collins, M. Walton, Transient analysis of carrier gas saturation in liquid source vapor generators, J. Vac. Sci. Technol. A 19 (1) (2001) 329–344.
[43] J.S. Jur, G.N. Parsons, Atomic layer deposition of Al_2O_3 and ZnO at atmospheric pressure in a flow tube reactor, ACS Appl. Mater. Interfaces 3 (2) (2011) 299–308.
[44] S. Salameh, J. Schneider, J. Laube, A. Alessandrini, P. Facci, J.W. Seo, L.C. Ciacchi, L. Mädler, Adhesion mechanisms of the contact interface of TiO_2 nanoparticles in films and aggregates, Langmuir 28 (31) (2012) 11457–11464.
[45] M.B.M. Mousa, C.J. Oldham, J.S. Jur, G.N. Parsons, Effect of temperature and gas velocity on growth per cycle during Al_2O_3 and ZnO atomic layer deposition at atmospheric pressure, J. Vac. Sci. Technol. A 30 (1) (2012) 01A155.
[46] N.A. Bailey, J.N. Hay, D.M. Price, A study of enthalpic relaxation of poly(ethylene terephthalate) by conventional and modulated temperature DSC, Thermochim. Acta 367–368 (0) (2001) 425–431.
[47] C.A. Wilson, R.K. Grubbs, S.M. George, Nucleation and growth during Al_2O_3 atomic layer deposition on polymers, Chem. Mater. 17 (23) (2005) 5625–5634.
[48] X. Liang, L.F. Hakim, G.D. Zhan, J.A. McCormick, S.M. George, A.W. Weimer, J.A. Spencer Ii, K.J. Buechler, J. Blackson, C.J. Wood, J.R. Dorgan, Novel processing to produce polymer/ceramic nanocomposites by atomic layer deposition, J. Am. Ceram. Soc. 90 (1) (2007) 57–63.
[49] R.T. Fenner, J.N. Reddy, Mechanics of Solids and Structures, second ed. CRC Press, 2012.
[50] S.-H. Jen, J.A. Bertrand, S.M. George, Critical tensile and compressive strains for cracking of Al_2O_3 films grown by atomic layer deposition, J. Appl. Phys. 109 (8) (2011) 084305.
[51] K. Nevalainen, R. Suihkonen, P. Eteläaho, J. Vuorinen, P. Järvelä, N. Isomäki, C. Hintze, M. Leskelä, Mechanical and tribological property comparison of melt-compounded nanocomposites of atomic-layer-deposition-coated polyamide particles and commercial nanofillers, J. Vac. Sci. Technol. A 27 (4) (2009) 929–936.
[52] M. Zarrelli, A.A. Skordos, I.K. Partridge, Investigation of cure induced shrinkage in unreinforced epoxy resin, Plast., Rubber Compos. 31 (9) (2002) 377–384.
[53] S.G. Hatzikiriakos, J.M. Dealy, Start-up pressure transients in a capillary rheometer, Polym. Eng. Sci. 34 (6) (1994) 493–499.
[54] D.C. Miller, R.R. Foster, S.-H. Jen, J.A. Bertrand, S.J. Cunningham, A.S. Morris, Y.-C. Lee, S.M. George, M.L. Dunn, Thermo-mechanical properties of alumina films created using the atomic layer deposition technique, Sens. Actuators, A 164 (1–2) (2010) 58–67.
[55] M.K. Tripp, C. Stampfer, D.C. Miller, T. Helbling, C.F. Herrmann, C. Hierold, K. Gall, S.M. George, V.M. Bright, The mechanical properties of atomic layer deposited alumina for use in micro- and nano-electromechanical systems, Sens. Actuators, A 130–131 (0) (2006) 419–429.